Chemical Science

ROYAL SOCIETY OF CHEMISTRY

EDGE ARTICLE

View Article Online
View Journal | View Issue

Cite this: *Chem. Sci.*, 2026, **17**, 5016

All publication charges for this article have been paid for by the Royal Society of Chemistry

"Impurity"-driven tunable organic room temperature phosphorescence *via* conformational regulation in multi host/guest systems

Arnab Dutta, [a] Utkarsh Singh, [b] Swapan K. Pati *[b] and Uday Maitra *[a]

The presence of trace amounts of impurities can have unprecedented effects on the luminescence features of organic room temperature phosphorescent (ORTP) materials, requiring conscientious investigation. In this study, we have compared the photoluminescence properties of biphenyl-4-carboxylic acid (**BCA**) and biphenyl-4,4′-dicarboxylic acid (**BDCA**), synthesized *via* two distinct synthetic routes—Friedel–Crafts (**FC-BCA** or **FC-BDCA**) and cross-coupling (**cc-BCA** or **cc-BDCA**) pathways and observed remarkable orange phosphorescence in **FC-BCA** or **FC-BDCA** which was absent in **cc-BCA** or **cc-BDCA**. Our investigations identified traces (<0.3 mol%) of diphenylbenzil based impurities, formed as byproducts during Friedel–Crafts acylation of biphenyl, responsible for the RTP activation in **FC-BCA** or **FC-BDCA**. Bicomponent solids prepared by deliberately doping traces of **DPB** into various organic matrices ensued tunable RTP color (green to red) with high quantum yield (26.4%) and a lifetime of up to 1.6 ms. Comprehensive experimental investigations substantiated with theoretical studies revealed that photoexcited conformational dynamics of guest **DPB** are responsible for RTP color variation concertedly involving multiple energy transfer channels, *e.g.*, singlet-to-singlet (SSET) and triplet-to-triplet (TTET). It presents a novel trace doping strategy for developing RTP materials with tunable optical features by synergistically controlling the ground and excited state geometries of a single guest molecule, which is rarely reported in the literature. Furthermore, by employing a suitable host matrix, we successfully stabilized a linear conformer of guest **DPB** in the ground state, which is otherwise unstable, and resulted in improved quantum yield. Simultaneously, we report unusual RTP from commercial **BDCA**, which we suspect to be caused by the presence of diphenylbenzil-based impurities, reiteratively emphasizing the importance of exercising caution whenever a system exhibits unusual properties.

Received 21st October 2025
Accepted 12th January 2026

DOI: 10.1039/d5sc08129g

rsc.li/chemical-science

Introduction

In recent years, purely organic room temperature phosphorescent (ORTP) materials have attracted tremendous attention as a sustainable alternative to their metal-based counterparts. Owing to their low cost, ease of modulation, and lower toxicity, they find potential applications in a wide variety of fields like organic light-emitting diodes (OLEDs),[1] bioimaging,[2] anti-counterfeiting technology,[3] *etc*. However, the realization of RTP from organic materials is a challenging task due to lower population of triplet excitons attributable to inefficient intersystem crossing (ISC) resulting from weak spin–orbit coupling.[4] Besides, triplet excitons are susceptible to quenching induced by molecular motion and triplet oxygen. As a result, there has been a long-standing belief that RTP from organic molecules can only be observed under inert conditions and at cryogenic temperatures. In the past few years, significant advancements have been made in this area through various strategies *e.g.* crystallization,[5] matrix rigidification,[6] heavy atom incorporation,[7] host/guest systems,[8] singlet-triplet energy modulation,[9] *etc.* to realize and engineer ORTP emission, circumventing the obstacles. However, seldom was any focus given to the purity (or impurity) profile of such materials. Traces of impurity can have unprecedented influence on the characteristics of a material.[10] Optical properties, especially phosphorescence, are very sensitive to the composition of materials which has been known since the early twentieth century.[11] However, concerns about the existence of impurities have been largely overlooked due to strenuous separation and characterization of trace impurities, and lack of adequate mechanistic understanding. Lately, the investigation on the effect of impurities has gained pace and several earlier reports on ORTP have been revisited. The credit goes to the advancement of analytical and characterization techniques that the origin and structures of the trace impurities have been successfully elucidated, which led to a valid interpretation of the observed luminescence, or even, in some

[a]*Department of Organic Chemistry, Indian Institute of Science, Bengaluru 560012, Karnataka, India. E-mail: maitra@iisc.ac.in*

[b]*Theoretical Sciences Unit, School of Advanced Materials (SAMat), Jawaharlal Nehru Centre for Advanced Scientific Research, Bengaluru 560064, Karnataka, India. E-mail: pati@jncasr.ac.in*

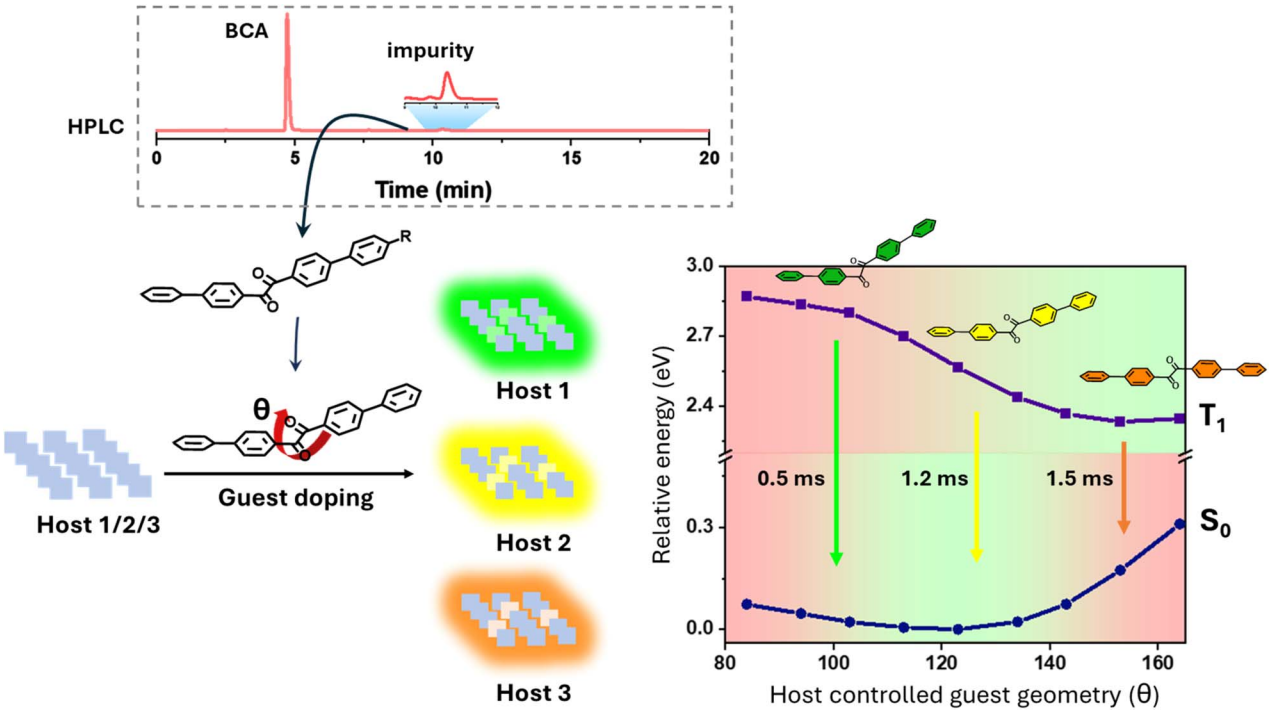

Scheme 1 Schematic representation of tunable RTP in a multi host/guest system by guest geometry control.

instances, disapproved the earlier interpretation of observation.[12] For instance, in 2021, the Liu group revealed the inconsistency in the photophysical properties of carbazole and some of its derivatives derived from two different sources, *i.e.*, commercial and lab synthesized carbazole.[12a] Detailed investigation revealed an isomeric impurity, benzoindole, responsible for unusual RTP in commercial carbazole and subsequent derived materials. This remarkable finding invalidated many earlier reports and interpretations provided for the observed RTP from carbazole derivatives. In a similar study, the Marder group rejected an earlier report that claimed to observe RTP from crystalline boric acid, and rather indicated it to be stemming from an unidentified impurity.[12b] More recently, the Hudson group showed a handful of arylboronic esters emitting persistent RTP as the crude product, which disappeared after purification.[12h] All these reports demonstrate the dramatic impact of trace impurities on RTP, hence emphasizing careful evaluation of sample composition. Nevertheless, they enriched our understanding of RTP mechanisms, providing valuable insights into designing new ORTP materials.

In this work, unusual RTP from biphenyl-4-carboxylic acid (**BCA**) and biphenyl-4,4′-dicarboxylic acid (**BDCA**), obtained from the reaction of biphenyl with oxalyl chloride under Friedel–Crafts conditions, is reported. Notably, **BCA** obtained from a commercial source (**com-BCA**) or synthesized in the lab (**cc-BCA**) following other procedures did not show any RTP. On the other hand, commercial **BDCA** (**com-BDCA**) exhibited similar RTP, which intensified upon crystallization. However, the **BDCA** synthesized in the lab from a cross-coupling (**cc-BDCA**) reaction did not show any such delayed luminescence. These exciting observations prompted us to investigate the origin of RTP in biphenyl-4-carboxylic acid (**FC-BCA**) and biphenyl-4,4′-dicarboxylic acid (**FC-BDCA**) obtained from the Friedel–Crafts reaction, and **com-BDCA**. We contemplated common impurities that might be present in both **FC-BCA** and **FC-BDCA**, possibly generated during the Friedel–Crafts reaction. After a strenuous analysis, impurities were indeed detected, which were characterized to be diphenylbenzil (**DPB**) and its derivative (**DPB-COOH**) (Scheme 1). Furthermore, to confirm the observation, we independently synthesized **DPB** in the lab to carry out further investigations. When **DPB** was doped into pure **BCA** or **BDCA**, it induced very similar luminescence even at 0.005 mol% doping content. **DPB** itself exhibits RTP—but it is feeble in solution and intensifies upon crystallization with a concomitant increase in the lifetime to 0.24 ms. Interestingly, we noticed a considerable shift in the RTP profiles in solution and in the crystalline state, attributable to its propensity for excited state conformational dynamics due to differential geometrical preferences in the ground and excited states, as revealed by theoretical studies. Furthermore, a strong dihedral angle (between the α-carbonyls) dependence of the RTP emission color was predicted, which led us to screen different host matrices to concertedly control the ground and excited state geometries of **DPB**, ensuing tunable RTP emission—green to orange red (Scheme 1). Simultaneously, we were able to stabilize the linear conformation of **DPB** at the ground state, which is otherwise unstable. As revealed by the detailed spectroscopic and theoretical studies, a rigid host matrix and host-to-guest energy transfer are the plausible attributes of the enhanced RTP performance in this dopant-based single-guest/multi-host system. In addition, our investigations indicate that the diphenyl-4,4′-dicarboxylic acid obtained from commercial

sources contains similar diphenylbenzil-based impurities, engendering RTP in **com-BDCA**.

Results and discussion

Friedel–Crafts reaction of biphenyl

In previous work from our group, we reported that biphenyl-4-carboxylic acid (**BCA**) sensitizes terbium (Tb^{3+}) and europium (Eu^{3+}) in terbium and europium cholate hydrogels, respectively, and we utilized those luminescent gels for various applications.[13] The dicarboxylic acid analogue, *i.e.*, biphenyl-4,4′-carboxylic acid (**BDCA**) has been extensively used for the synthesis of metal–organic frameworks (MOFs) including lanthanide (Ln)-based MOFs.[14] We intended to investigate Ln^{3+} sensitization mediated by **BDCA** within a supramolecular scaffold. Accordingly, we proceeded to synthesize **BDCA** following the Friedel–Crafts acylation pathway, wherein biphenyl was treated with oxalyl chloride (see the SI for details).[15] Subsequent column purification of the crude product led to the isolation of a compound (major fraction) which exhibited bright orange luminescence under UV light. The corresponding spectral measurement showed dual emission at 300–400 nm and 500–700 nm (Fig. 1). As depicted in Fig. 1d, NMR clearly indicated it to be biphenyl-4-carboxylic acid, hereinafter labelled as **FC-BCA**. We isolated another fraction, essentially a mixture of the desired compound **BDCA** (**FC-BDCA**) and **BCA** (**FC-BCA**), which also exhibited orange emission under UV light (Fig. S1).

Origin of delayed emission in FC-BCA

The steady-state photoluminescence spectra of **FC-BCA** exhibited dual emissions centered at 340 nm and 575 nm. However, when the luminescence was recorded in the time-gated mode with a delay time of 0.2 ms, only a structured emission centered at 575 nm was observed as the short-lived emission at 340 nm phased out (Fig. 2a). Gate-time dependent emission spectra further confirmed the long-lived nature of the lower energy emission (575 nm) with a lifetime of 1.34 ms (Fig. 2b and S2a). The decrease in luminescence intensity with an increase in temperature ascertained the phosphorescence nature of this delayed luminescence (Fig. 2c). Therefore, singlet and triplet emissions are most likely responsible for dual emissions at 340 nm and 575 nm, respectively. Surprisingly, the 575 nm emission was absent in samples procured from commercial sources (**com-BCA**) (Fig. 2d and e). However, a broad emission at 342 nm was indeed observed in the steady-state mode. Similarly, **BCA** synthesized (**cc-BCA**) by us from a coupling reaction exhibited a single emission band at 340 nm (Fig. S2b).

Therefore, we reasoned that the 340 nm emission of **FC-BCA** must be the intrinsic fluorescence of **BCA** and that the RTP at 575 nm was possibly caused by impurities.

To rationalize the origin of RTP in **FC-BCA**, it was indispensable to isolate and elucidate the structure of the impurity. Repeated column chromatography of **FC-BCA** did not improve the purity, which might be due to comparable R_f values of **BCA** and the impurity on the silica gel, or a strong intermolecular

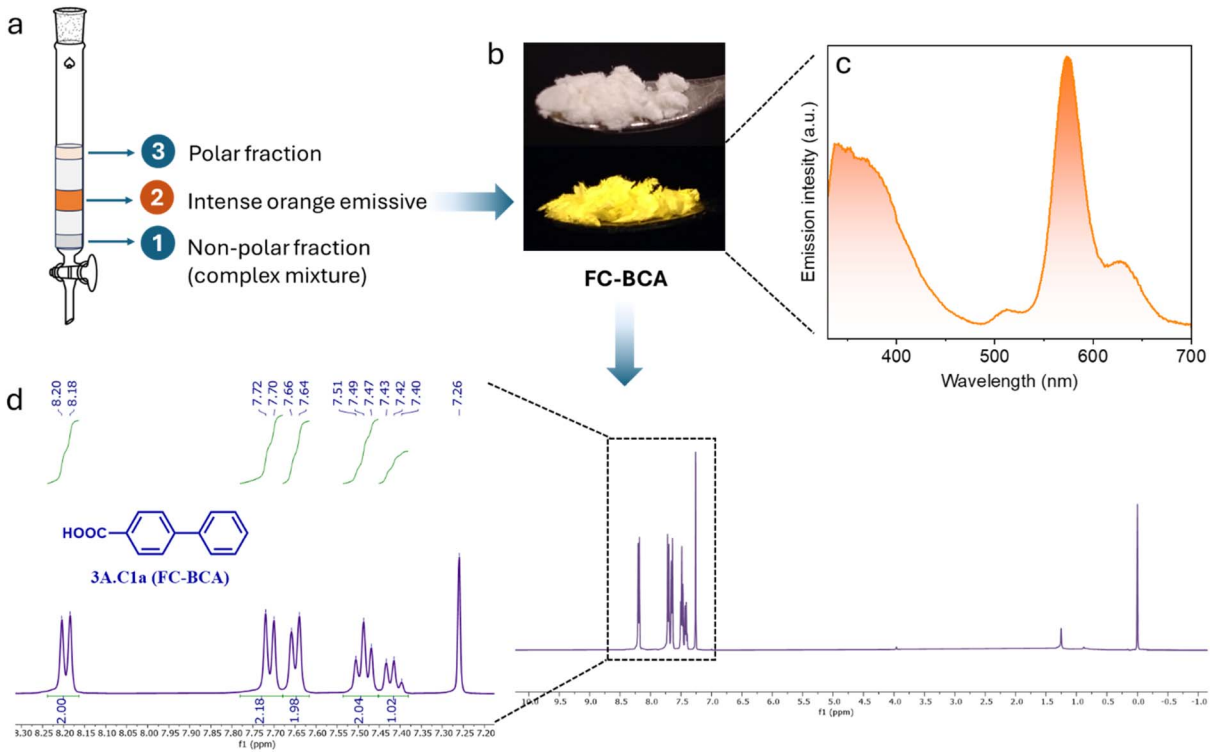

Fig. 1 (a) Illustration of the column purification of the yellowish crude product obtained from the Friedel–Crafts (FC) acylation of biphenyl with oxalyl chloride. (1) The non-polar fraction moved with the solvent front, (2) fraction that resulted in an intense orange emissive (when held under a UV lamp) material (**FC-BCA**), and (3) polar fraction, a weakly orange emissive solid. (b) Photographs of **FC-BCA** in ambient light (top) and under a UV lamp (bottom). (c) Steady-state emission spectra (λ_{ex} 315 nm) of **FC-BCA**. (d) ^{1}H NMR ($CDCl_3$, 400 MHz) of **FC-BCA**.

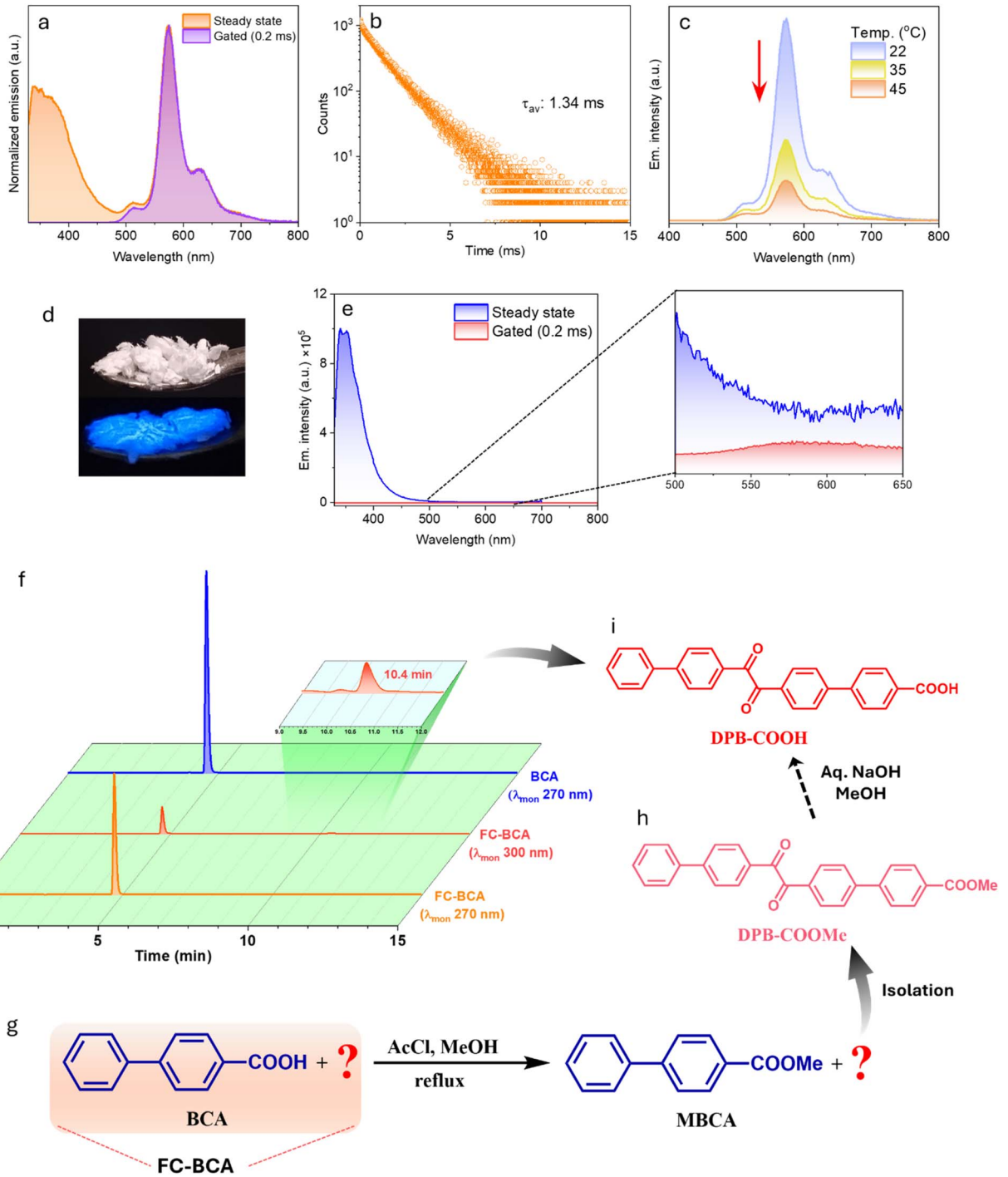

Fig. 2 (a) Steady-state and gated (gate/delay time: 0.2 ms) emission spectra (λ_{ex} 315 nm) of **FC-BCA**. (b) Emission decay profile of **FC-BCA** (λ_{ex} 315 nm; λ_{em} 575 nm). (c) Gated emission spectra (delay time: 0.2 ms; λ_{ex} 315 nm) of **FC-BCA** at different temperatures. (d) Photographs of pure **BCA** (crystallized commercial **BCA**) in ambient light (top) and under a UV lamp (bottom). (e) Steady-state and gated (gate time: 0.2 ms) emission spectra (λ_{ex} 315 nm) of commercial **BCA**. (f) HPLC chromatogram of **FC-BCA** and pure **BCA** (**cc-BCA**) (inset: zoomed trace for **FC-BCA** monitored at 300 nm) (solvent: 80% ACN-water with 0.2% AcOH). (g) Synthetic scheme for the esterification of **FC-BCA**. (h) Elucidated structure of the isolated impurity (**DPB-COOMe**). (i) Structure of **DPB-COOH**.

interaction between them. Moreover, the apparently clean NMR of **FC-BCA** was not informative (Fig. 1d), since a mere trace amount of a foreign impurity, undetectable by NMR, can be sufficient to activate RTP. Following several futile attempts, only during high-performance liquid chromatography (HPLC) analysis, we detected a weak peak corresponding to a 'foreign substance' at $t_R = 10.4$ min along with **BCA** ($t_R = 4.7$ min) when monitored at 300 nm (Fig. 2f).

It was hard to differentiate the impurity peak from the baseline when monitored at the λ_{max} of **BCA**, *i.e.*, 270 nm

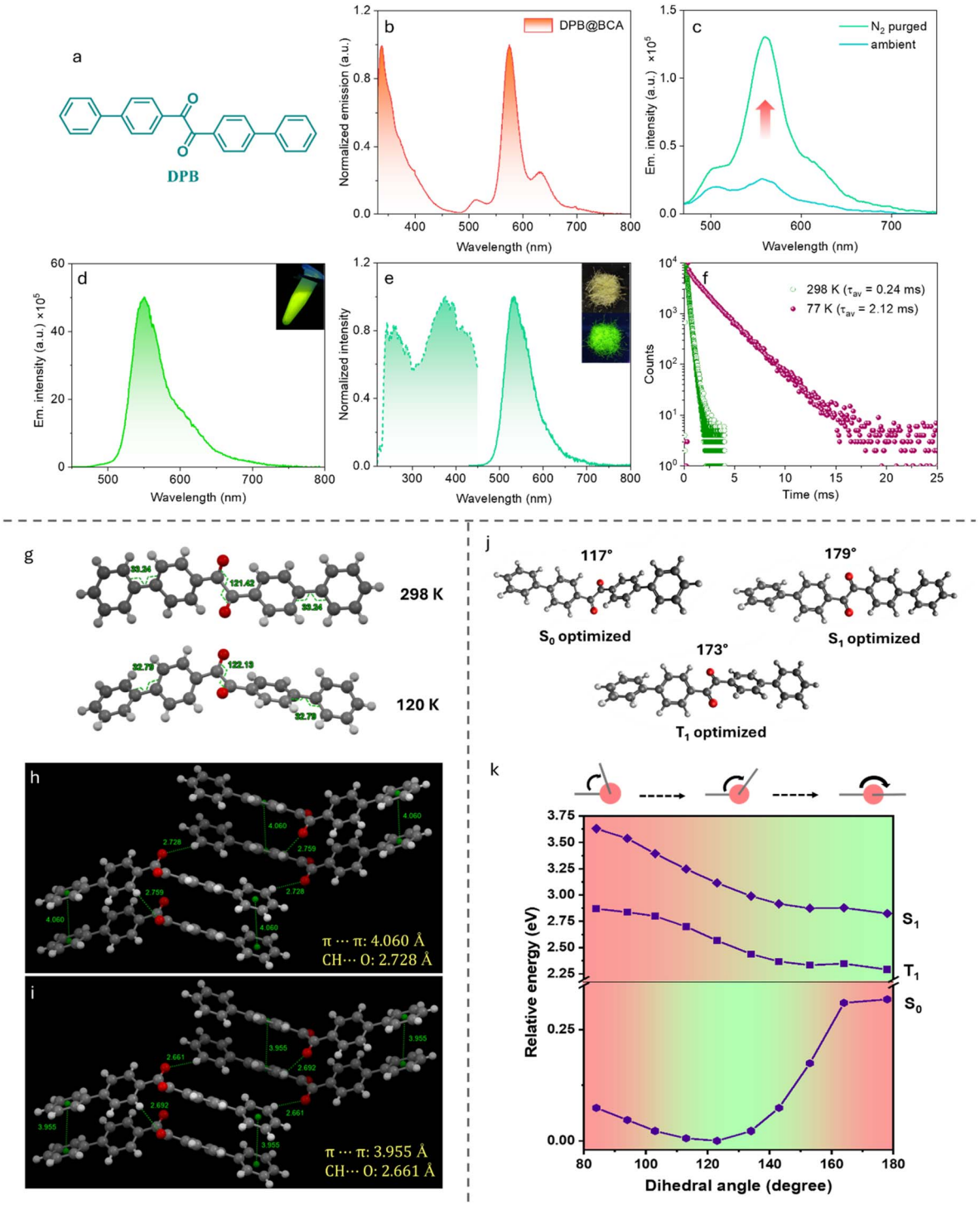

Fig. 3 (a) Structure of **DPB**. (b) Steady state emission (λ_{ex} 320 nm) spectrum of **DPB@BCA**. Steady state emission (λ_{ex} 310 nm) spectra of **DPB** (10 μM) in ACN at (c) 298 K and (d) 77 K (inset: photograph of the frozen solution under UV light). (e) Excitation (λ_{em} 535 nm) and emission (λ_{ex} 410 nm) spectra of crystalline **DPB** at room temperature (298 K) (inset: photograph of crystals in ambient light (top) and under UV light (bottom)). (f) Photoluminescence decay profile (λ_{ex} 410 nm; λ_{em} 535 nm) of crystalline **DPB** at 298 and 77 K. (g) Crystal structure of **DPB** deduced from SCXRD data obtained at 298 K and 120 K. Various intermolecular interactions with their respective interatomic distances in the **DPB** crystal at (h) 298 and (i) 120 K (calculated using Mercury[21] software). (j) Ground (S_0) and excited state (S_1 and T_1) optimized geometries of **DPB**. (k) Dihedral angle (between α-carbonyls) dependent potential energy curves of S_0, S_1 and T_1 states (relative to S_0 optimized geometry).

because of the red shifted absorption maxima of the impurity, as revealed by the photodetector array (PDA) detector of our HPLC system (Fig. S3). We collected HPLC fractions corresponding to the $t_R = 10.4$ min peak from multiple injections, but the recovered amount was too little (<1 mg) for subsequent characterization studies. However, the

bicomponent solid solution obtained from a mixture of pure **BCA** and the HPLC concentrate resulted in similar RTP, which was discernible in the time-gated spectrum (Fig. S4). Thus, this confirmed that the substance appearing at $t_R = 10.4$ min in the chromatogram was indeed responsible for RTP induction. In order to isolate the impurity from the bulk material, we esterified biphenyl-4-carboxylic acid by treating **FC-BCA** with MeOH under acidic conditions with the anticipation that methyl biphenyl-4-carboxylate would significantly differ in polarity from biphenyl-4-carboxylic acid as well as from the impurity and might lead to a better separation of the trace component (Fig. 2g). We indeed isolated an unknown compound in a minute amount (1.5 mg), which was characterized to be an unsymmetrical diphenylbenzil derivative (analytical data in SI, S5), **DPB-COOMe** (Fig. 2h). This led us to contemplate that the trace amount of the corresponding acid, *i.e.*, **DPB-COOH** which was present at a concentration of ~0.2 mol%, might be responsible for RTP induction in **FC-BCA**. Appearance of a peak at 10.4 min in the HPLC chromatogram of aq. KOH treated **DPB-COOMe**, resembling the one in **FC-BCA**, further confirmed our speculation (Fig. 2i and S6).

Symmetrical diphenylbenzil also induces RTP

Phosphorescence from benzil is known since the mid-twentieth century.[16] However, the phosphorescence intensity is very weak in solution at room temperature, attributable to the non-radiative deexcitation of the triplet state. In 2013, Gong *et al.* reported crystallization-induced room temperature phosphorescence from benzil and its derivatives, facilitated by the impediment of intermolecular motions in crystals.[17] We reasoned that the symmetrical diphenylbenzil (**DPB**) (Fig. 3a), like **DPB-COOH**, could also be formed in the reaction of biphenyl with oxalyl chloride and with it being less polar than **DPB-COOH** or **BCA**, likely gets eluted down with the initial fractions during the purification of the crude product on silica gel. To validate our assumption, we synthesized **DPB** in the lab and subjected it to HPLC studies along with the concentrated initial fractions, which were obtained during column purification of the Friedel–Crafts reaction crude product (Fig. 1a, sample 1; details in the SI). The presence of the **DPB** peak in the chromatogram of the concentrate confirmed its formation (Fig. S7). Interestingly, as depicted in Fig. 3b, **DPB** incorporated **BCA** (**DPB@BCA**) also exhibited intense RTP, similar to that of **DPB-COOH@BCA**. Therefore, diphenylbenzil and its derivatives engender remarkable RTP when doped into **BCA**, even in trace amounts (<0.5 mol%). Due to easier synthetic access to **DPB**, we considered **DPB** as our model compound for further investigations.

Photophysical properties of diphenylbenzil (DPB)

To comprehend the role of **DPB** in inducing RTP in the solid bicomponent mixture, we conducted a detailed photophysical investigation of **DPB**. **DPB** exhibits maximum absorption at 310 nm (Fig. S8a), considerably red-shifted compared to that of simple benzil[17] (λ_{abs} 260 nm). This shift in absorption maxima can be ascribed to the extended conjugation which stems from additional phenyl groups at the 4, 4′ position of the benzil unit. As illustrated in Fig. 3c, it exhibited a structured, weak emission in solution, centered at 560 nm with shoulders at 530 and 620 nm. The corresponding excitation maximum, observed at 310 nm, correlated well with its absorption profile (Fig. S8b). Upon purging the solution with N_2, a marked enhancement (~5-fold) in luminescence intensity was observed, attributable to the mitigation of triplet quenching by dissolved oxygen, thereby confirming the triplet origin of the emission (Fig. 3c). It is worth mentioning that no noticeable peak corresponding to singlet emission (fluorescence) was detected. Therefore, the observed emission is entirely of triplet origin.

When a solution of **DPB** in ACN was cooled to 77 K, an intense green emission was observed with an average lifetime of 17 ms (Fig. 3d and S9). As shown in Fig. 3d, the spectrum differed considerably from that obtained at room temperature with the λ_{max} moving from 560 nm to 550 nm. The remarkable increase in phosphorescence intensity and lifetime at 77 K very likely resulted from the restricted motion of **DPB** in a frozen solution. The observed shift in the phosphorescence profile possibly stems from the excited state conformational dynamics of the **DPB** molecule, a phenomenon known for benzil.[18] In the excited state, it adopts a flattened conformation with a larger dihedral angle between the carbonyls, whereas the ground state is thermodynamically more stable in a twisted geometry with a relatively smaller angle between the carbonyls (*vide infra*). Therefore, **DPB** emits from two distinct geometries in rigid (77 K) and non-rigid (298 K) environments, resulting in the observed spectral shift.

Unlike in solution, crystallized **DPB** exhibits intense perceivable RTP under UV light, with a lifetime of 0.24 ms (Fig. 3e). Except for a slight shift in the emission maximum, 535 and 550 nm in crystal and solution, respectively, the emission profile was found to be similar to that of the frozen solution (77 K), indicating that the emitting species have similar geometries in both the environments. However, the excitation profile was found to be broad, extending to 410 nm, possibly because of multiple intermolecular interactions in the crystal (Fig. 3e). Notably, when crystalline **DPB** was cooled to 77 K, the emission intensity further intensified with a concomitant increase in phosphorescence lifetime to 2.12 ms (Fig. 3f) implying that at ambient temperature the molecules in the crystal still possessed some residual motion.

Single crystal analysis

To understand the molecular packing and intermolecular interactions in the crystalline state, single crystal X-ray diffraction (SCXRD) analysis of **DPB** was carried out at room temperature (298 K, CCDC 2427014) and low temperature (120 K, CCDC 2427013). As illustrated in Fig. 3g, **DPB** adopts a twisted geometry with the α-dicarbonyls oriented at 122° with respect to each other. The phenyl groups of the biphenyl moiety are positioned in different planes, forming a dihedral angle of 32° and intermolecularly stacked along the *b* axis (Fig. S10). The crystal parameters and geometries were similar at both temperatures (Table S1 and Fig. 3g). However, the extent of intermolecular interactions was

noticeably different (Fig. 3h and i). For example, at 77 K, the closest non-bonding distance between carbonyl-O and aromatic-H is 2.661 Å, which is smaller than the sum of their van der Waals radii (O: 1.52 Å; H: 1.20 Å), suggesting a stronger C–H···O interaction. At 298 K, the same distance is 2.728 Å, pointing at a weaker C–H···O interaction. Similarly, at lower temperature the π···π interaction arising from the stacked phenyl rings with a spacing of 3.995 Å is stronger than that at room temperature, where the phenyl rings are 4.060 Å apart. Furthermore, we generated Hirshfeld[19] surfaces to visualize the extent of various intermolecular interactions (Fig. S11). The red contours on the Hirshfeld surface close to the carbonyl oxygen indicated a strong C–H···O interaction at low temperature. Therefore, the decrease in various interatomic distances with a concomitant drop in cell volume and increase in density implies that as temperature decreases, the crystal packing becomes more compact, resulting in stronger intermolecular interactions (Table S1). This explains the increase in the phosphorescence intensity and lifetime at 77 K.

Theoretical investigations

In order to understand the photoexcitation dynamics of **DPB**, we conducted theoretical investigations. The ground (S_0) state geometry was optimized by density functional theory (DFT) using the B3LYP exchange-correlation functional and 6–31 + g(d) basis set and the excited (S_1 & T_1) states were optimized by TDDFT using the CAM-B3LYP exchange–correlation functional and 6–31 + g(d) basis set. As depicted in Fig. 3j, S_0 has a twisted geometry with the carbonyls oriented at 117°; whereas the excited state is thermodynamically more stable in a flattened conformation (~173°). Furthermore, the dihedral angle dependent potential energy curves for S_0, S_1 and T_1 clearly demonstrate a differential conformational preference in the ground and excited states (Fig. 3k). Therefore, the shift in the phosphorescence profile of the dilute solution of **DPB** at 298 K and 77 K stems from two distinct geometries of the emitting species. At 298 K, the free molecules in the solution quickly relax to a flattened or linear geometry post photoexcitation and emit lower energy photons. While at 77 K, when molecular motions are restricted in the frozen state, **DPB** is forced to emit from the S_0 optimized geometry, resulting in a blue-shifted emission profile.

The natural transition orbital (NTO) analysis of the S_0–T_1 transition in S_0 (117°), T_1 (173°) and crystal geometries (122°) revealed that the holes and electrons are localized over the carbonyls with a strong n–π* nature of the S_0–T_1 transition (Fig. S12). Strong n–π* nature and high SOCME $\langle T_1|\hat{H}_{SO}|S_0\rangle$ between S_0–T_1 further explained the observed RTP in **DPB**. Furthermore, we looked at the oscillator strengths, relative energies of S_n and T_n, and the corresponding SOC matrix elements at different geometries. The oscillator strengths, summarized in Table S2, indicate that the experimental absorption maxima at 310 nm arise from the S_0–S_3 transition (π–π*), and the absence of emission from singlet state (fluorescence) is attributable to small oscillator strength (10^{-3}–10^{-4}) for the S_0–S_1 transition. Additionally, there exist multiple triplet states below S_1, with high S_1–T_n SOC. The NTO analysis of these states shows a change in the nature of the transition from n–π* in the case of S_1 to π–π* for T_2/

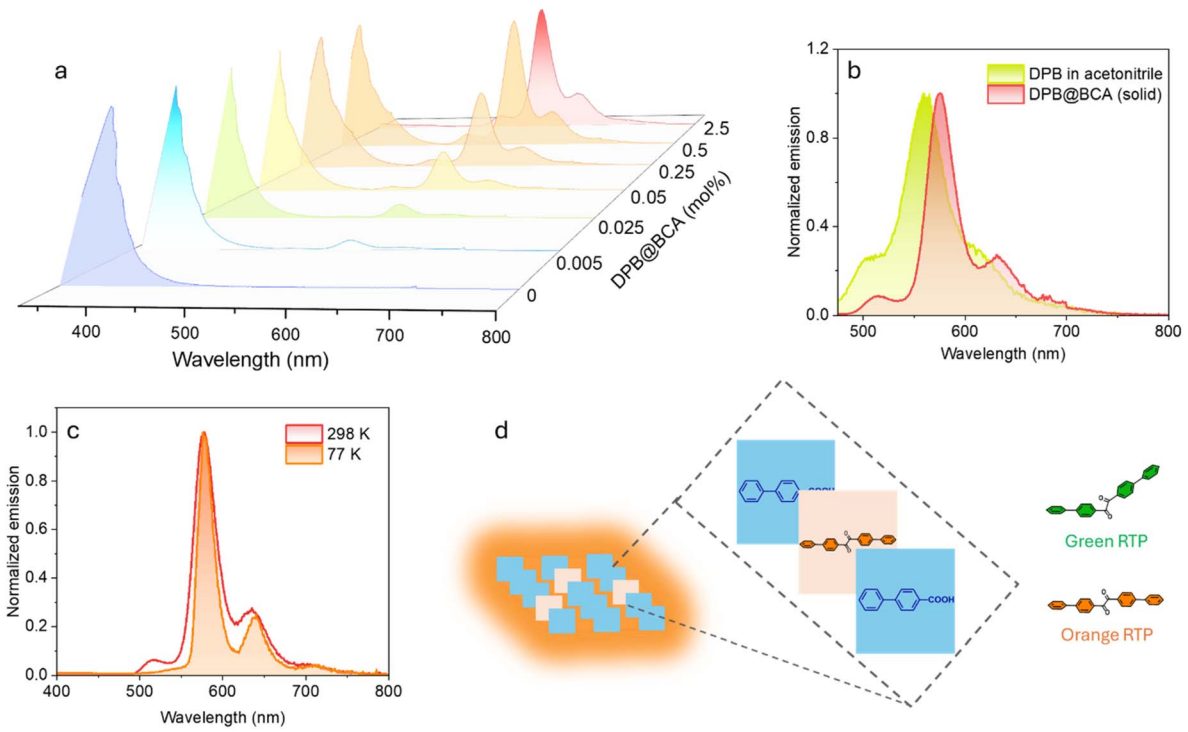

Fig. 4 (a) Steady-state emission spectra (λ_{ex} 320 nm) of **DPB@BCA** at various dopant concentrations. (b) Photoluminescence spectra of **DPB** in ACN (298 K) and a **BCA** solid matrix. (c) Photoluminescence spectra (λ_{ex} 360 nm) of 0.5 mol% **DPB@BCA** at 298 and 77 K. (d) Schematic representation of guest incorporation inside the **BCA** matrix. Photoluminescence measurement at cryogenic temperature indicates that **DPB** adopts a linear conformation inside **BCA**.

T_3 which follows El-Sayed's rule[20] for enhanced ISC (Fig. S13). This opens ISC channels to populate the triplet state; S_1 to T_2 being the most probable pathway with high SOCME (>20 cm^{-1}). Therefore, the negligible oscillator strength of the S_0–S_1 transition, presence of multiple ISC channels and strong T_1/S_0 SOC promote efficient triplet emission.

Mechanism of RTP from DPB@BCA

With a comprehensive understanding of conformational dynamics of guest diphenylbenzil, we delved into detailed photophysical studies of **DPB@BCA**, prepared by externally doping diphenylbenzil in biphenyl-4-carboxylic acid, to elucidate the underlying mechanism of RTP in trace 'impurity' doped **BCA**. **BCA** doped with variable mol% of the guest was prepared by solvent evaporation from solutions of **BCA** containing variable amounts of **DPB**. As depicted in Fig. 4a, even 0.005 mol% of **DPB** induced observable RTP, which increased with the dopant concentration. Upon excitation at 320 nm, emission peaks at 340 nm, 515 nm, 575 nm and 635 nm emerged in the steady state photoluminescence spectrum, where the higher energy emission (340 nm) corresponds to host fluorescence. While in the time-gated mode, only peaks at 515 nm, 575 nm and 635 nm were seen, as the short-lived host fluorescence phased out within the applied gate window (Fig. S14a). The delayed emission resembled that of **DPB** in solution at room temperature (Fig. 4b), indicating the guest origin of the observed luminescence, with a lifetime of 1.5 ms (Fig. S14b).

The corresponding excitation (λ_{em} 575) spectrum exhibited a broad signature, with multiple local maxima at 320, 360 and 490 nm (Fig. S15a). However, the RTP profile was independent of the excitation wavelength (Fig. S15b), as well as remained unchanged irrespective of the guest concentration.

There are several reports where the origin of RTP in the host–guest system has been attributed to the crystal defects induced by the trace amounts of guests.[12a,c,12g] However, no noticeable changes in the powder X-ray diffraction (PXRD) patterns for pristine **BCA** and 0.5 mol% **DPB@BCA** ruled out any morphological effect in our system (Fig. S16). Next, we carried out a detailed analysis of the RTP lifetime to extract more information. RTP decay profiles were obtained at different excitation and emission wavelengths. Interestingly, a comparable lifetime (1.4–1.5 ms) was observed in all combinations irrespective of dopant concentration (Table S3). Therefore, emissions at 515, 575 and 635 nm must originate from the same electronic state. Moreover, a single exponential decay indicates that the emission takes place from an exclusive molecular species/geometry, and no other competitive pathway is involved.

We arbitrarily chose a 0.5 mol% guest-doped system to conduct subsequent studies. We investigated the emission at a cryogenic temperature (77 K). To our surprise, it ensued orange emission, which was in sharp contrast to **DPB** in solution as it was green luminescent at cryogenic temperature. Spectral measurements revealed that the emissions at 77 K and 298 K were identical (Fig. 4c). However, the luminescence lifetime increased to 2.3 ms which followed a single exponential decay, ascertaining the triplet nature of the emission (Fig. S17). Therefore, unlike in the solution, **DPB** does not undergo any conformational change upon photoexcitation when incorporated into the **BCA** matrix. **DPB** seems to have a fixed geometry and the position of the RTP peak at 575 nm indicates that it most likely adopts a linear geometry (with the carbonyls oriented at about ~173°) in the host matrix (Fig. 4d). Therefore, the **BCA** matrix selectively stabilizes a flattened conformation of **DPB** in the ground state; otherwise, the flattened conformation is thermodynamically stable only in the excited state, as manifested by theoretical and solution state studies. We scrutinized the excitation and absorption spectra of the host and guest@host to understand the mechanism of RTP, revealing an excellent correlation between the absorption and excitation spectra (Fig. S18). Interestingly, the spectral features of **DPB@BCA** RTP excitation (λ_{em} 575 nm), which is extended till 520 nm, is similar to **BCA** fluorescence (λ_{em} 340 nm) in the lower wavelength region, say to 320 nm (Fig. S18). Therefore, it is likely that under higher energy excitation, the host absorbs energy and relays it to the guest *via* energy transfer (ET), singlet-to-singlet (SSET) or triplet-to-triplet (TTET), with its feasibility being substantiated by the relatively higher S_n and T_n energy levels of **BCA** compared to those of **DPB** (Table S4 and Fig. S19). To be certain about the ET mechanism, the fluorescence lifetime of **BCA** was determined with and without the dopant.

The fluorescence lifetime of pristine **BCA** is itself too short (1.38 ns) to reliably be compared with that of the doped system. Nevertheless, a decrease in host lifetime was observed with an increase in guest concentration—the average lifetime dropped to 0.98 ns in 2.8 mol% **DPB@BCA**, indicating host-to-guest SSET under higher energy excitation (Fig. S20). However, the contribution of TTET cannot be ruled out in this case.

Furthermore, the spread of the RTP excitation profile to a longer wavelength, 330–500 nm, might result from the direct excitation of the guest or the presence of a charge transfer band. Like in a solution where **DPB** is in a molecularly dispersed state, a guest doped at such a lower concentration, *e.g.*, 0.5 mol%, will be similarly dispersed inside the host–guest solid solution. However, unlike in solution, **DPB** exists in a linear conformation in the **BCA** matrix that may give rise to the observed bathochromic shift in excitation/absorption. TDDFT calculation indeed suggested a slightly different absorption profile for the linear conformation of **DPB** where the simulated spectrum of the linear conformer is about 30 nm shifted from that of the twisted conformer (Fig. S21). However, none of them have any significant absorption beyond 400 nm. Since neither **BCA** nor **DPB** absorbs beyond 400 nm, we reasoned that the broad low-intensity excitation band centered at 490 nm emerges from the charge transfer transition. Theoretical investigations unveiled the presence of a mixed state consisting of both charge transfer (CT) and local excitations (LE), which is characteristic for a one-to-one host–guest complexation (Fig. 5a). According to TDDFT calculation, the peak at 490 nm can be assigned to a mixed (CT + LE) state, with singlet and triplet energies of 2.39 eV and 1.83 eV, respectively (Fig. S22). It is worth reiterating that as evident from the experimental data, RTP emission originates exclusively from the guest triplet state (^3LE_G), irrespective of the excitation wavelength. Therefore, at higher energy excitation (HEE), the matrix absorbs the excitation energy

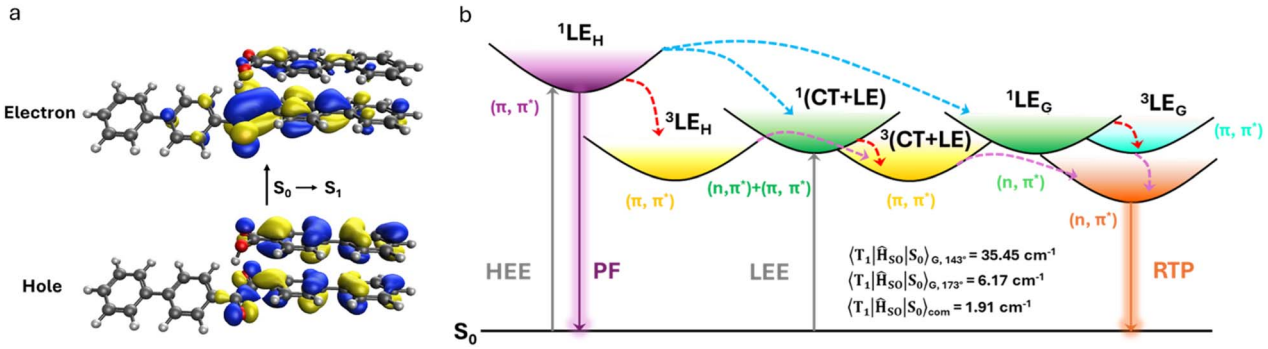

Fig. 5 (a) NTO ($S_0 \rightarrow S_1$) of **BCA** and the **DPB** complex showing formation of the mixed state, exhibiting of charge transfer (CT) and local excitation (LE) characteristics. (b) Simplified Jablonski diagram illustrating various photophysical events leading to RTP in **DPB@BCA** solid solution. Solid and dashed (cyan: SSET, purple: TTET, and red: ISC) arrows represent radiative and non-radiative transitions, respectively. The absence of any noticeable emission from the mixed state can be attributed to its poor value of SOCME (T_1/S_0) compared to that of guest **DPB** (linear conformer of **DPB** is considered as **DPB** adopts a flattened geometry in the **BCA** matrix).

and relays it to the guest, whereas lower energy (LEE) irradiation induces a CT transition which in turn feeds the closely positioned LE_G, resulting in guest-centered emission (Fig. 5b).

RTP color tuning by the multi-host/guest strategy

The conformational variability in **DPB** and its influence on luminescence provides an opportunity to modulate the RTP color by synergistically controlling the ground and excited state geometries through a multi-host strategy. The remarkable RTP from **DPB@BCA** further encouraged us to explore other aromatic hosts. We chose biphenyl (**BiPh**), benzophenone (**BP**), benzoic acid (**BA**) and naphthalene (**NaPh**) due to the conducive positioning of their T_1 relative to **DPB**, which can potentially facilitate host-to-guest TTET, resulting in enhanced RTP (Fig. 6a). We also included poly(methyl methacrylate) (PMMA) as a non-aromatic polymeric host. All the hosts were recrystallized, and the purity was ascertained by HPLC before proceeding with the study (Fig. S23a). **Guest@host** materials can be prepared by solvent evaporation or the melt-casting method (details provided in the SI). To carry out a comprehensive investigation, we prepared 0.5 mol% **DPB** embedded materials and formation of solid solutions was confirmed by differential scanning calorimetry (DSC) measurements (Fig. S23b). The bicomponent solids exhibited RTP with variable emission color, ranging from green in PMMA to orange red in naphthalene (Fig. 6b). A similarity in the PXRD patterns of the pristine host and **guest@host** eliminates any influence of crystal defects on the observed RTP (Fig. S24). Instead, the conformation of the emitting species, *i.e.*, **DPB**, seems to determine the emission color. A systematic spectroscopic investigation was carried out to rationalize the host dependency of RTP. Bicomponent materials containing aromatic hosts showed two sets of peaks in the steady-state photoluminescence spectra—emission at a shorter wavelength (300–400 nm) corresponds to intrinsic host emission, whereas the lower energy structured emission at 490–630 nm was similar to **DPB** emission in solution, suggesting that the emission at room temperature takes place from a linear conformation of **DPB** (Fig. S25). However, the PMMA matrix resulted in green RTP (540 nm), similar to that of crystalline **DPB**. Therefore, the intramolecular motion of **DPB** is strictly restricted in PMMA and forced to emit from a twisted conformer, ensuing green RTP. The Commission Internationale de l'Éclairage (CIE) plot of the RTP emission demonstrates host-dependent tunable emission from green to orange-red (Fig. 6c). The RTP lifetime varied (within a short range) across different host matrices—0.46 ms in **BP** to 1.45 ms in **BCA** (Table S5). Notably, the **BiPh** host resulted in a maximum quantum yield (Φ_{RTP}) of 26.4% (Table S6).

Luminescence measurement at 77 K shed light on the geometry of **DPB** embedded in different host matrices (details in SI, Fig. S25). Briefly, in benzoic acid and the benzophenone host, it adopts a twisted geometry and experiences enough flexibility to undergo excited state conformational relaxation, as evident from distinct emissions at ambient and cryogenic temperatures. Therefore, they ensure a sufficiently rigid environment to activate guest RTP, but not enough to restrict geometrical relaxation. However, **DPB** is stabilized in a liner conformation inside the biphenyl matrix, as evident from identical phosphorescence profiles and mono-exponential luminescence decay. Therefore, biphenyl (**BiPh**) behaved like biphenyl-4-carboxylic acid (**BCA**), which may be attributed to the common biphenyl functionality in both the hosts. In contrast to other bicomponent materials, **DPB@NaPh** exhibited excitation-dependent dual emission at 77 K. When excited at 420 nm, emission at 530 nm dominated, whereas 365 nm excitation resulted in a structured emission centered at 580 nm. We reasoned that the volatility of naphthalene exposed the surface **DPB** molecules that no longer experienced matrix stabilization and eventually adopted a twisted conformation. On the other hand, **DPB** in the bulk host is stabilized in a linear geometry. The presence of two molecular species results in an excitation-dependent dual emission at 77 K—emission at 530 nm originating from the aggregated **DPB** molecules at the host surface, whereas **DPB** dispersed in the bulk host emits at 580 nm (see the SI for a detailed discussion). Thorough analysis of RTP excitation profiles of all the host–guest materials highlights some common features. For instance, a part of the RTP excitation spectra, high energy excitation, resembles the fluorescence excitation of the pristine host, implying RTP sensitization

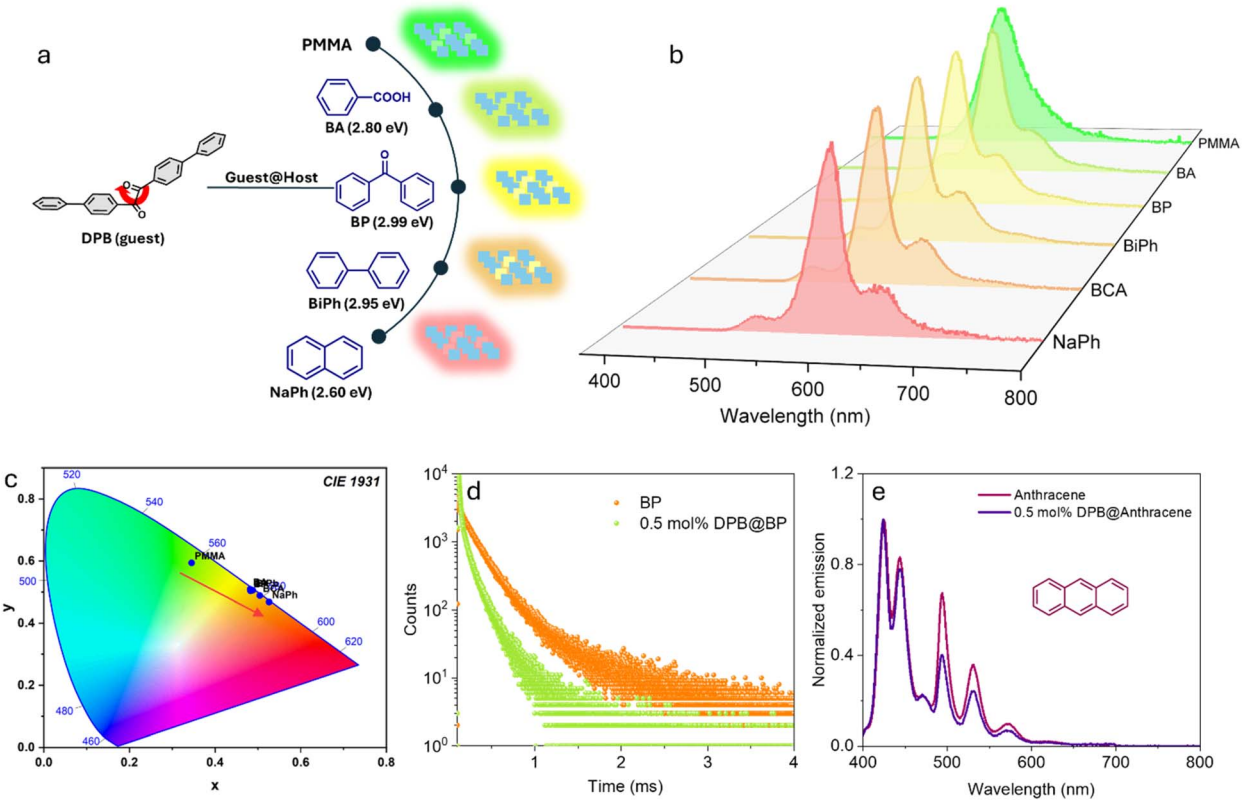

Fig. 6 (a) Schematic representation of guest doping into multiple hosts (respective T_1 energy[22] is mentioned within parentheses). (b) RTP profile (gate time: 0.2 ms) of guest@host (guest concentration: 0.5 mol% in aromatic hosts and 1 wt% in PMMA) with various hosts. (c) Commission Internationale de l'Éclairage (CIE)-1931 plot of the RTP from 0.5 mol% **DPB@BA/BP/NaPh/BiPh/BCA** and 1 wt% **DPB@PMMA**. (d) Photoluminescence decay profiles (λ_{ex} 380 nm; λ_{em} 417 nm; monitoring the host emission lifetime) of **BP** and 0.5 mol% **DPB@BP**. (e) Steady-state photoluminescence spectra (λ_{ex} 380 nm) of anthracene and 0.5 mol% **DPB**@anthracene (inset: structure of anthracene).

through host-to-guest energy transfer. On the other hand, lower energy excitation directly excites the embedded guest molecules. As described earlier, the decrease in **BCA** fluorescence lifetime and the conducive positioning of its triplet state strongly indicated ET processes. In a similar study, we compared the phosphorescence lifetime of benzophenone (**BP**) with and without guest doping. We monitored the phosphorescence decay at 417 nm to minimize interference from the guest emission. As shown in Fig. 6d, the phosphorescence lifetime of **BP** dropped from 0.35 ms in the pristine host to 0.19 ms in 0.5 mol% **DPB@BP**, attributable to the host-to-guest triplet-to-triplet energy transfer (TTET). Furthermore, to validate the role of host triplet energy, we selected a host with its T_1 lying below that of **DPB**, which would potentially quench the guest emission. We considered anthracene as its T_1 (1.83 eV) is energetically lower than that of **DPB** in either of the extreme geometries, twisted or linear. As anticipated, no distinguishable guest emission emerged from **DPB@anthracene** (Fig. 6e), clearly demonstrating that the properties of these bicomponent materials are strongly influenced by the host triplet energy. Moreover, we explored acyclic acids like palmitic acid and succinic acid as host matrices, but the emission was very weak, with Φ_{RTP} <1% for 0.5 mol% **DPB**-embedded materials (Fig. S26). Therefore, suitable aromatic hosts that can effectively restrict molecular motion and sensitize guest emission are necessary to activate RTP. We also investigated the stability of the doped systems, which ranges from weeks to months and depends on the host material. For example, the solid solutions in **BCA**, **BiPh** and **NaPh** were found to be stable for at least two months, whereas those in **BP** and **BA** were stable for 2–3 weeks when stored at 4 °C.

Unusual RTP in com-BDCA

Commercial biphenyl-4,4′-dicarboxylic acid (**com-BDCA**) is usually produced by a Friedel–Crafts reaction that proceeds *via* benzil type intermediates.[15b] Therefore, it is plausible that **com-BDCA** may contain trace amounts of diphenylbenzil derivatives. We were curious to investigate the emission profiles of **BDCA** obtained from commercial sources (Aldrich and Fluka). As shown in Fig. 7a and S27a, **com-BDCA** exhibited an intense and broad fluorescence, with a maximum at 400 nm, in the steady-state mode, but no distinct lower energy (~570 nm) emission peak. However, when the spectra were obtained with a 0.2 ms gate-time, weak emissions at 515, 570 and 625 nm were observed. The positions of the peaks were comparable to the RTP emissions of our lab-prepared bicomponent materials with a lifetime of ~1.3 ms (Fig. 7b and S27b). Therefore, RTP in **com-BDCA** is discernible only in the time-gated mode as intense

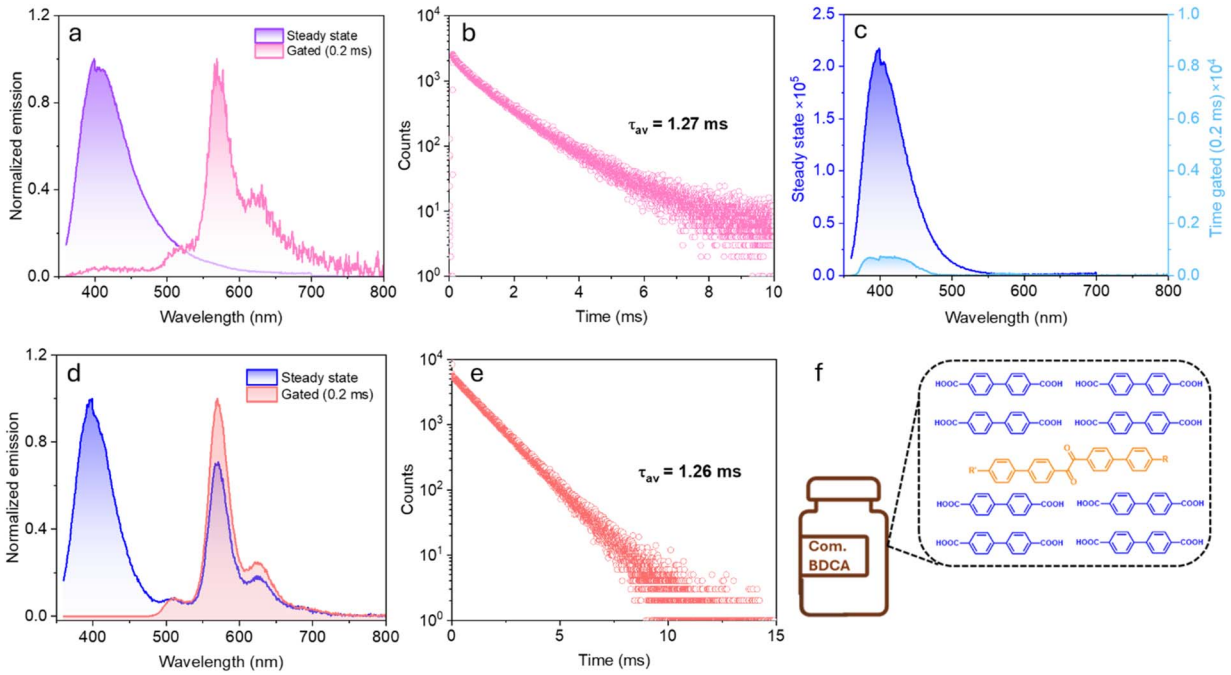

Fig. 7 (a) Photoluminescence spectra (λ_{ex} 340 nm) and (b) RTP decay profile (λ_{ex} 340 nm; λ_{em} 570 nm) of commercial **BDCA** (Aldrich). (c) Photoluminescence spectra of lab synthesized BDCA (**cc-BDCA**). (d) Emission (λ_{ex} 340 nm) and (e) RTP decay profile (λ_{ex} 340 nm; λ_{em} 570 nm) of 0.1 mol% **DPB**-embedded pure BDCA (**cc-BDCA**). (f) Schematic representation of the diphenylbenzil-based impurity in commercial **BDCA**.

BDCA fluorescence, which shadows the weak phosphorescence, phases out within the applied gate window. Furthermore, to prove that the source of this weak RTP is some impurity in the commercial samples, we synthesized **BDCA** in the lab *via* a cross-coupling reaction (**cc-BDCA**), which did not show any noticeable emission at around 570 nm, not even in gated spectra (Fig. 7c). However, just like **com-BDCA**, intrinsic fluorescence with λ_{max} at 400 nm can be observed in the steady-state spectrum. Next, we embedded **DPB** in **cc-BDCA**. Interestingly, it activated the RTP with emission peaks at 515, 570 and 625 nm, which even showed up in the steady-state spectrum, with a lifetime of 1.4 ms (Fig. 7d and e). Therefore, the RTP in **com-BDCA** must be induced by some trace impurities, very likely by diphenylbenzil based impurities (Fig. 7f). Unfortunately, despite several attempts, we could not detect any potential impurities by HPLC (Fig. S28), possibly because the concentration was too small to detect, and it requires <0.01 mol% of DPB to activate RTP. Nevertheless, we crystallized **com-BDCA** to increase its purity. Surprisingly, the RTP intensity increased upon crystallization (Fig. S29), which can be attributed to the ordered arrangements of **BDCA** molecules that efficiently impeded molecular motion of the impurities incorporated in the crystals.

Conclusions

In conclusion, this exploratory research describes how the comparison between two different sources of biphenyl-4-carboxylic acid (**BCA**), synthesized from two different synthetic routes in combination with strenuous analytical exercise, led us to successfully isolate and characterize trace impurities that engendered remarkable RTP in organic matrices. Diphenylbenzil (**DPB**) and its derivatives activate intense and tunable RTP in organic matrices even at < 0.1 mol% concentrations, facilitated by simple mixing such as solvent evaporation or melt-casting. The comparison of luminescence properties at cryogenic and ambient temperatures, host luminescence lifetimes, DSC and XRD analysis complemented with TDDFT studies shed light on the mechanism of RTP in bicomponent solid solutions, which suggested that the observed RTP was purely of guest origin. However, multiple energy transfer pathways, such as SSET or TTET and the generation of mixed states (CT + LE), have been elucidated, leading to enhanced RTP performance. The variation in RTP color is attributed to the host controlled photoexcited conformational dynamics of dipenylbenzil, revealing a novel approach for developing RTP materials with tunable optical features by concertedly controlling the ground and excited state geometries of a single guest molecule. Notably, with a careful selection of the host environment, we could selectively stabilize the linear geometry of **DPB** at the ground state, which is otherwise infeasible, resulting in good quantum efficiency for lower energy RTP. This easy-to-prepare, trace ingredient doping strategy represents a facile way of designing RTP materials with high efficiency, tunability and low-cost, which can find potential applications in time resolved (bio)imaging, multicolor display, information encryption, *etc*. During our investigation, Chen *et al.* reported two benzil derivatives, 4,4′-dimethylbenzil and 4,4′-di-*tert*-butylbenzil, exhibiting cyan to yellow RTP in different polymeric hosts, where some of them stabilized the ground sate geometry of the phosphor.[23] However, unlike our present studies, no selective stabilization of the linear geometry

was reported, resulting in poor RTP quantum yield for lower energy emission.

Our investigation simultaneously raises suspicion regarding the purity of biphenyl-4,4′-dicarboxylic acid obtained from commercial sources (**com-BDCA**). We showed that **com-BDCA** exhibits RTP which is absent in lab-synthesized **BDCA** (**cc-BDCA**), strongly indicating the presence of benzil-based impurities. However, the identity of the impurities remains elusive. In line with the growing concerns on the impact of impurities on RTP emission, our finding reiteratively emphasizes the conscientious analysis of sample purity and being apprehensive about the justification forwarded to explain the observation, especially when a system exhibits unusual properties.

Author contributions

A. D. carried out all the experimental work. U. S. performed theoretical calculations. S. K. P. and U. M. supervised the project. A. D. wrote the initial draft. U. S., S. K. P. and U. M. edited the manuscript. All authors have given approval to the final version of the manuscript.

Conflicts of interest

There are no conflicts to declare.

Data availability

CCDC 2427013 and 2427014 contain the supplementary crystallographic data for this paper.[24a,b]

All the experimental and computational data are provided in the supplementary information (SI). Supplementary information is available. See DOI: https://doi.org/10.1039/d5sc08129g.

Acknowledgements

UM thanks the SERB, Govt. of India for the award of a J.C. Bose fellowship (SR/S2/JCB-68/2007) and a research grant (CRG/2020/001140). SKP thanks SERB, DST and acknowledges a JC Bose Fellowship for financial support. AD thanks MoE, Govt. of India for a PMRF fellowship. US thanks JNCASR for a fellowship. AD thanks Kishorkumar Sindogi (central X-ray facility, IISc), Gayathri Govind V (JNCASR), and Poulomi Mukherjee (IISc) for their assistance in solving the crystal structure, luminescence measurement at cryogenic temperature and TCSPC measurement, respectively. UM and AD sincerely thank Prof. Subi J. George (JNCASR) and Prof. Mahesh Hariharan (IISERTVM) for their insightful discussion and suggestions. The authors thank CCMS and NSM PARAM Yukti, JNCASR for computational facilities. The authors thank Indian Science Technology and Engineering facilities Map (I-STEM), a program supported by the Office of the Principle Scientific Adviser to the Govt. of India, for enabling access to the X-ray facility at the Indian Institute of Science, Bangalore, to carry out XRD measurements.

Notes and references

1 (*a*) R. Nagata, K. Goushi, H. Nakanotani and C. Adachi, in *Organic Electronics Materials and Devices*, ed. S. Ogawa, Springer Japan, Tokyo, 2024, DOI: 10.1007/978-4-431-56936-7_2, pp. 73–118; (*b*) H. Shi, W. Yao, W. Ye, H. Ma, W. Huang and Z. An, *Acc. Chem. Res.*, 2022, **55**, 3445–3459; (*c*) J. Yang, M. Fang and Z. Li, *Acc. Mater. Res.*, 2021, **2**, 644–654.

2 (*a*) Q. Miao, C. Xie, X. Zhen, Y. Lyu, H. Duan, X. Liu, J. V. Jokerst and K. Pu, *Nat. Biotechnol.*, 2017, **35**, 1102–1110; (*b*) L. Yang, M. Zhao, W. Chen, J. Zhu, W. Xu, Q. Li, K. Pu and Q. Miao, *Angew. Chem., Int. Ed.*, 2023, **63**, e202313117; (*c*) Y. Zhang, H. Li, M. Yang, W. Dai, J. Shi, B. Tong, Z. Cai, Z. Wang, Y. Dong and X. Yu, *Chem. Commun.*, 2023, **59**, 5329–5342; (*d*) X. Dai, Z. Liu, Y. Ge and P. Wei, *Trends Anal. Chem.*, 2023, **168**, 117339; (*e*) F. Xiao, H. Gao, Y. Lei, W. Dai, M. Liu, X. Zheng, Z. Cai, X. Huang, H. Wu and D. Ding, *Nat. Commun.*, 2022, **13**, 186.

3 H. Chen, X. Yao, X. Ma and H. Tian, *Adv. Opt. Mater.*, 2016, **4**, 1397–1401.

4 S. Hirata, *Adv. Opt. Mater.*, 2017, **5**, 1700116.

5 (*a*) W. Zhao, Z. He and B. Z. Tang, *Nat. Rev. Mater.*, 2020, **5**, 869–885; (*b*) W. Z. Yuan, X. Y. Shen, H. Zhao, J. W. Y. Lam, L. Tang, P. Lu, C. Wang, Y. Liu, Z. Wang, Q. Zheng, J. Z. Sun, Y. Ma and B. Z. Tang, *J. Phys. Chem. C*, 2010, **114**, 6090–6099; (*c*) C.-R. Wang, Y.-Y. Gong, W.-Z. Yuan and Y.-M. Zhang, *Chin. Chem. Lett.*, 2016, **27**, 1184–1192; (*d*) J. Yang, X. Zhen, B. Wang, X. Gao, Z. Ren, J. Wang, Y. Xie, J. Li, Q. Peng, K. Pu and Z. Li, *Nat. Commun.*, 2018, **9**, 840.

6 (*a*) X. Yan, H. Peng, Y. Xiang, J. Wang, L. Yu, Y. Tao, H. Li, W. Huang and R. Chen, *Small*, 2022, **18**, e2104073; (*b*) Y. Su, S. Z. F. Phua, Y. Li, X. Zhou, D. Jana, G. Liu, W. Q. Lim, W. K. Ong, C. Yang and Y. Zhao, *Sci. Adv.*, 2018, **4**, eaas9732; (*c*) H. Wu, W. Chi, Z. Chen, G. Liu, L. Gu, A. K. Bindra, G. Yang, X. Liu and Y. Zhao, *Adv. Funct. Mater.*, 2019, **29**, 1807243.

7 (*a*) Z. Mao, Z. Yang, Y. Mu, Y. Zhang, Y. F. Wang, Z. Chi, C. C. Lo, S. Liu, A. Lien and J. Xu, *Angew. Chem., Int. Ed.*, 2015, **54**, 6270–6273; (*b*) J. Wang, X. Gu, H. Ma, Q. Peng, X. Huang, X. Zheng, S. H. P. Sung, G. Shan, J. W. Y. Lam, Z. Shuai and B. Z. Tang, *Nat. Commun.*, 2018, **9**, 2963; (*c*) O. Bolton, K. Lee, H. J. Kim, K. Y. Lin and J. Kim, *Nat. Chem.*, 2011, **3**, 205–210.

8 (*a*) D. Li, F. Lu, J. Wang, W. Hu, X. M. Cao, X. Ma and H. Tian, *J. Am. Chem. Soc.*, 2018, **140**, 1916–1923; (*b*) Z. Y. Zhang, Y. Chen and Y. Liu, *Angew. Chem., Int. Ed.*, 2019, **58**, 6028–6032; (*c*) Z. Xie, X. Zhang, H. Wang, C. Huang, H. Sun, M. Dong, L. Ji, Z. An, T. Yu and W. Huang, *Nat. Commun.*, 2021, **12**, 3522.

9 (*a*) X. Chen, C. Xu, T. Wang, C. Zhou, J. Du, Z. Wang, H. Xu, T. Xie, G. Bi, J. Jiang, X. Zhang, J. N. Demas, C. O. Trindle, Y. Luo and G. Zhang, *Angew. Chem., Int. Ed.*, 2016, **55**, 9872–9876; (*b*) A. A. Kongasseri, S. Garain, S. N. Ansari, B. C. Garain, S. M. Wagalgave, U. Singh, S. K. Pati and S. J. George, *Chem. Mater.*, 2023, **35**, 7781–7788; (*c*)

S. Garain, S. N. Ansari, A. A. Kongasseri, B. Chandra Garain, S. K. Pati and S. J. George, *Chem. Sci.*, 2022, **13**, 10011–10019.

10 (*a*) K. Yasui, *Materials*, 2023, **16**, 1612; (*b*) X. Chen, C. Li, Y. Xu, A. Dolocan, G. Seward, A. Van Roekeghem, F. Tian, J. Xing, S. Guo, N. Ni, Z. Ren, J. Zhou, N. Mingo, D. Broido and L. Shi, *Chem. Mater.*, 2021, **33**, 6974–6982; (*c*) Y. Wang, J. Su, Z. Lin, J. Zhang, J. Chang and Y. Hao, *J. Mater. Chem. C*, 2022, **10**, 13395–13436; (*d*) C. L. Briant, *Mater. Manuf. Process.*, 2000, **15**, 155–156.

11 (*a*) D. B. Clapp, *J. Am. Chem. Soc.*, 1939, **61**, 523–524; (*b*) C. S. Bilen, N. Harrison and D. J. Morantz, *Nature*, 1978, **271**, 235–237; (*c*) P. Xue, P. Wang, P. Chen, B. Yao, P. Gong, J. Sun, Z. Zhang and R. Lu, *Chem. Sci.*, 2017, **8**, 6691.

12 (*a*) C. Chen, Z. Chi, K. C. Chong, A. S. Batsanov, Z. Yang, Z. Mao, Z. Yang and B. Liu, *Nat. Mater.*, 2020, **20**, 175–180; (*b*) Z. Wu, J. C. Roldao, F. Rauch, A. Friedrich, M. Ferger, F. Würthner, J. Gierschner and T. B. Marder, *Angew. Chem., Int. Ed.*, 2022, **61**, e202200599; (*c*) B. Ding, L. Ma, Z. Huang, X. Ma and H. Tian, *Sci. Adv.*, 2021, **7**, eabf9668; (*d*) C. Chen, K. C. Chong, Y. Pan, G. Qi, S. Xu and B. Liu, *ACS Mater. Lett.*, 2021, **3**, 1081–1087; (*e*) K. C. Chong, C. Chen, C. Zhou, X. Chen, D. Ma, G. C. Bazan, Z. Chi and B. Liu, *Adv. Mater.*, 2022, **34**, 2201569; (*f*) W. Qiao, M. Yao, J. Xu, H. Peng, J. Xia, X. Xie and Z. a. Li, *Angew. Chem., Int. Ed.*, 2023, **62**, e202315911; (*g*) H. Xiao, D. S. Zheng, L. Y. Zhang, L. J. Xu and Z. N. Chen, *Adv. Funct. Mater.*, 2023, **33**, 2214241; (*h*) Z. Wu, C. Herok, A. Friedrich, B. Engels, T. B. Marder and Z. M. Hudson, *J. Am. Chem. Soc.*, 2024, **146**, 31507–31517.

13 (*a*) A. Dutta and U. Maitra, *ACS Sens.*, 2022, **7**, 513–522; (*b*) A. Dutta, S. Mukherjee, J. Haldar and U. Maitra, *ACS Sens.*, 2024, **9**, 351–360.

14 (*a*) B. Fernández, G. Beobide, I. Sánchez, F. Carrasco-Marín, J. M. Seco, A. J. Calahorro, J. Cepeda and A. Rodríguez-Diéguez, *CrystEngComm*, 2016, **18**, 1282–1294; (*b*) W. Zhang, H. Yin, Z. Yu, X. Jia, J. Liang, G. Li, Y. Li and K. Wang, *Nanomaterials*, 2022, **12**, 2062; (*c*) X. Fan, S. Wang, M. Pan, H. Pang and H. Xu, *ACS Energy Lett.*, 2024, **9**, 2840–2847.

15 (*a*) A. J. Gosselin, G. E. Decker, B. W. McNichols, J. E. Baumann, G. P. A. Yap, A. Sellinger and E. D. Bloch, *Chem. Mater.*, 2020, **32**, 5872–5878; (*b*) Zhongwei National Engineering Research Center for Coking Technology Co. Ltd, *China Pat.*, CN103483186A, 2014.

16 (*a*) D. J. Morantz and A. J. C. Wright, *J. Chem. Phys.*, 1971, **54**, 692–697; (*b*) D. S. Roy, K. Bhattacharyya, S. C. Bera and M. Chowdhury, *Chem. Phys. Lett.*, 1980, **69**, 134–140.

17 Y. Gong, Y. Tan, H. Li, Y. Zhang, W. Yuan, Y. Zhang, J. Sun and B. Z. Tang, *Sci. China Chem.*, 2013, **56**, 1183–1186.

18 (*a*) A. K. Singh, D. K. Palit and J. P. Mittal, *Chem. Phys. Lett.*, 2002, **360**, 443–452; (*b*) K. Maduwantha, S. Yamada, K. R. Koswattage, T. Konno and T. Hosokai, *Materials*, 2020, **13**, 3904.

19 M. A. Spackman and D. Jayatilaka, *CrystEngComm*, 2009, **11**, 19–32.

20 M. A. El-Sayed, *J. Chem. Phys.*, 1963, **38**, 2834–2838.

21 C. F. Macrae, I. Sovago, S. J. Cottrell, P. T. A. Galek, P. McCabe, E. Pidcock, M. Platings, G. P. Shields, J. S. Stevens, M. Towler and P. A. Wood, *J. Appl. Crystallogr.*, 2020, **53**, 226–235.

22 (*a*) P. J. S. Gomes, C. Serpa and L. G. Arnaut, *J. Photochem. Photobiol., A*, 2006, **184**, 228–233; (*b*) S. Jhulki, T. J. Chow and J. N. Moorthy, *New J. Chem.*, 2016, **40**, 6854–6859; (*c*) S. Kuno, H. Akeno, H. Ohtani and H. Yuasa, *Phys. Chem. Chem. Phys.*, 2015, **17**, 15989–15995; (*d*) Y. Han, X. Luo, R. Lai, Y. Li, G. Liang and K. Wu, *J. Phys. Chem. Lett.*, 2019, **10**, 1457–1463.

23 Z. Chen, X. Chen, D. Ma, Z. Mao, J. Zhao and Z. Chi, *J. Am. Chem. Soc.*, 2023, **145**, 16748–16759.

24 (*a*) CCDC 2427013: Experimental Crystal Structure Determination, 2026, DOI: 10.5517/ccdc.csd.cc2mghrc; (*b*) CCDC 2427014: Experimental Crystal Structure Determination, 2026, DOI: 10.5517/ccdc.csd.cc2mghsd.